

RESEARCH ARTICLE

Analysis of COVID-19 epidemic with intervention impacts by a fractional operator

Sanjay Bhattar ^a, Sangeeta Kumawat ^a, Bhamini Bhatia ^a, Sunil Dutt Purohit ^{b,c*}

^aDepartment of Mathematics, Malaviya National Institute of Technology Jaipur, India

^bDepartment of HEAS (Mathematics), Rajasthan Technical University, Kota, India

^cDepartment of Computer Science and Mathematics, Lebanese American University, Beirut, Lebanon
sbhattar.maths@mnit.ac.in, 00sangeetakumawat@gmail.com, bhaminibhatia56@gmail.com,
sunil_a_purohit@yahoo.com

ARTICLE INFO

Article History:

Received 4 January 2024

Accepted 23 March 2024

Available Online 24 July 2024

Keywords:

COVID-19

Intervention measures

Caputo fractional derivative

Normalized sensitivity index

Numerical simulations

AMS Classification 2010:

92D30; 34A08; 26A33; 93A30

ABSTRACT

This study introduces an innovative fractional methodology for analyzing the dynamics of COVID-19 outbreak, examining the impact of intervention strategies like lockdown, quarantine, and isolation on disease transmission. The analysis incorporates the Caputo fractional derivative to grasp long-term memory effects and non-local behavior in the advancement of the infection. Emphasis is placed on assessing the boundedness and non-negativity of the solutions. Additionally, the Lipschitz and Banach contraction theorem are utilized to validate the existence and uniqueness of the solution. We determine the basic reproduction number associated with the model utilizing the next generation matrix technique. Subsequently, by employing the normalized sensitivity index, we perform a sensitivity analysis of the basic reproduction number to effectively identify the controlling parameters of the model. To validate our theoretical findings, numerical simulations are conducted for various fractional order values, utilizing a two-step Lagrange interpolation technique. Furthermore, the numerical algorithms of the model are represented graphically to illustrate the effectiveness of the proposed methodology and to analyze the effect of arbitrary order derivatives on disease dynamics.



1. Introduction

In the realm of infectious diseases, mathematical modeling stands as a pivotal tool, offering insights into the spread and control mechanisms. The foundations of this discipline were laid in 1927 by Kermack and Mc Kendrick, who introduced a fundamental compartment model for complex epidemic studies in epidemiology [1]. In the contemporary world, heightened attention has been directed towards research on an array of epidemic diseases like HIV, Malaria, Dengue, HBV, posing significant challenges in containment and prevention of disease within the human population. As the world grapples with these pre-existing health concerns, a new,

unprecedented threat emerged on the horizon in late 2019, named COVID-19, originating in Wuhan, China. This novel coronavirus rapidly escalated into a pandemic, challenging our understanding of disease transmission and intervention strategies. Although, the exact origins of the virus remains elusive, it is believed to have originated from animals and potentially transmitted to humans through intermediaries such as SARS-CoV and MERS-CoV. COVID-19 manifests with a range of symptoms, from the typical fever, dry cough, and fatigue to severe respiratory distress with some cases being asymptomatic. During the pandemic, individuals infected with the coronavirus could

*Corresponding Author

spread it even without displaying the symptoms, constituting an incubation period of ranging from 2 to 14 days [2]. In the absence of a specific treatment for the first year of its emergence, non-pharmaceutical interventions took precedence such as isolation, mask-wearing, sanitization, and stringent restrictions on public gatherings. Governments around the world imposed lockdowns, constituting one of the largest quarantines in history, to curb the virus's spread. Consequently, understanding the role of different intervention strategies in transmission control remains a vital research focus. Several compartmental models analyzing the effect of various intervention strategies for COVID-19 have been proposed. In the study conducted by [3], a model was introduced to analyze the COVID-19 outbreak in China (Shanxi province). The researchers investigated the impact of the city lockdown date on the ultimate case count. They discovered that an earlier lockdown in the city could significantly reduce the number of infectious cases. Another study by [4], focused on the COVID-19 pandemic in the U.S.A, analyzing the impacts of non-pharmaceutical strategies. Additionally, [5] formulated a mathematical model to analyze the spread of COVID-19 in India. Their findings highlighted the significance of strict isolation measures for susceptible individuals, which could effectively bring down the rate of contact between susceptible and infected persons.

Nowadays, Fractional calculus is emerging as a vital branch of mathematics, extending traditional calculus by including integrals and derivatives with non-integer orders, enabling a more nuanced analysis of epidemic dynamics, originating from Leibniz's inquiry in 1695 [6]. Over the past three decades, researchers have delved into a range of fractional derivatives, such as Riemann-Liouville, Caputo, Caputo-Fabrizio, Atangana-Baleanu and more, captivated by their usage in diverse domains, including science, biology, economics, and engineering. Unlike traditional integer-order models focusing solely on the current state, fractional order models incorporate memory and hereditary effects, integrating past information to make more accurate epidemic predictions. Current advancements in epidemiological research emphasize the significance of utilizing models incorporating fractional order derivatives. A study investigated the behavior of HCV (Hepatitis C virus) disease, employing a mathematical model incorporating differential equations (DEs) of fractional-order. This

model accounted for two crucial transmission components: interactions between the virus and cells, and the rate at which infected cells are cured, as presented in [7]. Also, in a study [8] researchers investigated the dynamics of COVID-19 transmission in Ethiopia, emphasizing on different age classes of infected population. The researchers employed Chebyshev polynomials to transform a fractional system into a set of algebraic equations. Additionally, [9] introduced an epidemic model of fractional order, integrating the classical Atangana-Baleanu-Caputo operator and Caputo operator, to investigate COVID-19 transmission. Considering these instances, it becomes apparent that employing fractional order derivatives in modeling real-life situations produces more precise outcomes than integer order scenarios. This statement finds support by a multitude of research investigations [10–16] in the field. In particular, Caputo fractional derivative (CFD) has found widespread application in various epidemic models, underscoring its utility. This significance is particularly evident when dealing with constant functions, as the Caputo derivative of such functions yields zero. The Caputo operator plays a pivotal role in solving ordinary differential equations, involving a subsequent fractional integral to achieve the desired order of fractional derivative. Notably, the Caputo fractional differential equation allows for the inclusion of local initial conditions in the model derivation process. Numerous researchers have successfully employed the Caputo operator to model diverse real-life scenarios, as evidenced by the literature [17–21].

Consequently, we emphasize the continued application of the Caputo operator in our current work, building upon the successful endeavors of previous researchers. This study investigates the dynamics of COVID-19 model considering the effect of intervention strategies introduced by [22]. By utilizing the CFD, our objective is to grasp the memory effect and non-local behavior essential for understanding the dynamics of COVID-19 infection. The choice of CFD lies in its capability to incorporate local primary conditions and enhance the accuracy of the model. The paper is structured in the described manner: Section 2 delves into fundamental mathematical concepts essential for the subsequent discussions. Section 3 describe the formulation and examination of the extension of COVID-19 model utilizing the CFD. In Section 4, we explore the non-negativity and boundedness of the model, accompanied by an exploration of

the existence and uniqueness of solution for the given model. Section 5 determines the basic reproduction number and conducts a sensitivity analysis concerning each parameter. Section 6, presents a numerical simulation employing a two-step Lagrange interpolation method to validate the theoretical findings. Section 7, showcases the results and discussion. Finally, in Section 8, we draw conclusions from the entire study.

2. Preliminaries

Within this part, we will define some basic notations and definitions related to fractional calculus, that will be extensively utilized in this paper.

Definition 1. Let $\phi : (0, \infty) \rightarrow \mathbb{R}$ be a function, then the Riemann-Liouville fractional integral operator [6] with order $\alpha > 0$ is expressed as:

$${}^c_0\mathcal{I}_t^\alpha \phi(t) = \frac{1}{\Gamma(\alpha)} \int_0^t \frac{\phi(s)}{(t-s)^{\alpha-1}} ds; \quad t \geq 0, \quad (1)$$

here, $\Gamma(\cdot)$ referred as a well-known Gamma function.

Definition 2. Let $\phi : (0, \infty) \rightarrow \mathbb{R}$ be a function, then the CFD [6] with order $\alpha > 0$ is represented as

$${}^c_0\mathcal{D}_t^\alpha \phi(t) = \begin{cases} \frac{1}{\Gamma(\mathbf{n} - \alpha)} \int_0^t \frac{\phi^n(s)}{(t-s)^{\alpha+1-\mathbf{n}}} ds; \\ \quad \alpha \in (\mathbf{n} - 1, \mathbf{n}), \\ D_t^\mathbf{n} \phi(t); \quad \alpha = \mathbf{n}, \end{cases} \quad (2)$$

where, $t \geq 0$ and \mathbf{n} is any positive integer. When $\alpha \in (0, 1)$,

$${}^c_0\mathcal{D}_t^\alpha \phi(t) = \frac{1}{\Gamma(\mathbf{n} - \alpha)} \int_0^t \frac{\phi'(s)}{(t-s)^\alpha} ds. \quad (3)$$

Also, the corresponding fractional integral with order ($\alpha > 0$) is described as

$${}^c_0\mathcal{I}_t^\alpha \phi(t) = \frac{1}{\Gamma(\alpha)} \int_0^t \frac{\phi(s)}{(t-s)^{\alpha-1}} ds; \quad \Re(\alpha) > 0. \quad (4)$$

Definition 3. The Laplace transform(LT) [9] of the CFD with order $\alpha > 0$ is expressed as:

$$\begin{aligned} \mathcal{L} [{}^c_0\mathcal{D}_t^\alpha \phi(t)] (\mathfrak{s}) &= \mathfrak{s}^\alpha \mathcal{L} [\phi(t)] \\ &- \sum_{m=0}^{\mathbf{n}-1} \phi^{(m)}(0) \mathfrak{s}^{\alpha-m-1}, \end{aligned} \quad (5)$$

where, $\alpha \in (\mathbf{n} - 1, \mathbf{n}]$ and $\mathbf{n} \in \mathbb{N}$.

Definition 4. The Mittag-Leffler function [23] characterized by two parameters is expressed as

$$E_{a,b}(\mathcal{S}) = \sum_{r=0}^{\infty} \frac{\mathcal{S}^r}{\Gamma(r a + b)}, \quad (6)$$

where, $a, b > 0$ and also, $E_{a,1}(\mathcal{S}) = E_a(\mathcal{S})$. The LT of one parameter Mittag-Leffler function can be expressed as follows:

$$\begin{aligned} \mathcal{L} [1 - E_a(-kt^a)] &= \frac{k}{\mathfrak{s}(\mathfrak{s}^a + k)}, \\ \mathcal{L} [E_a(-kt^a)] &= \frac{\mathfrak{s}^a}{\mathfrak{s}(\mathfrak{s}^a + k)}. \end{aligned} \quad (7)$$

3. Formulation of Mathematical Model

Within this part, we develop a fractional-order epidemic model by applying the CFD operator to the classical integer-order model of COVID-19, as described in [22]. The COVID-19 integer-order model is defined by the given set of nonlinear ordinary DEs:

$$\begin{aligned} \frac{dS(t)}{dt} &= (1 - \rho)\Omega - \beta S(A + I) - (\mu + \lambda)S + \zeta Q_1, \\ \frac{dQ_1(t)}{dt} &= \rho\Omega - \sigma\beta Q_1(A + I) + \lambda S - (\mu + \zeta)Q_1, \\ \frac{dA(t)}{dt} &= \beta S(A + I) + \sigma\beta Q_1(A + I) \\ &\quad - (q_1 + q_2 + \mu)A, \\ \frac{dQ_2(t)}{dt} &= q_1 A - (q_3 + q_4 + \mu)Q_2, \\ \frac{dI(t)}{dt} &= q_3 Q_2 + q_2 A + (\delta + \mu + \gamma)I, \\ \frac{dT(t)}{dt} &= \gamma I - (\mu + \eta)T, \\ \frac{dR(t)}{dt} &= q_4 Q_2 + \eta T - \mu R, \end{aligned} \quad (8)$$

with initial conditions

$$\begin{aligned} S(0) &= S_0 > 0, Q_1(0) = Q_{1,0} \geq 0, A(0) = A_0 \geq 0, \\ Q_2(0) &= Q_{2,0} \geq 0, I(0) = I_0 \geq 0, \\ T(0) &= T_0 \geq 0, R(0) = R_0 \geq 0. \end{aligned} \quad (9)$$

Here, the entire population $\mathbb{P}(t)$ is segmented to seven sub-population compartments, say $S(t)$, $A(t)$, $Q_1(t)$, $Q_2(t)$, $T(t)$, $I(t)$, and $R(t)$ where the total population is sum of these compartments as:

$$\begin{aligned} \mathbb{P}(t) &= S(t) + Q_1(t) + A(t) + Q_2(t) + I(t) \\ &\quad + T(t) + R(t). \end{aligned} \quad (10)$$

When an individual is in good health but can contract the infection is susceptible (S), Susceptible individuals under quarantine due to lockdown measures are comprising in (Q_1), those

in the community who exhibit no symptoms yet are in incubation period are categorized as Asymptomatic (A), those asymptomatic individuals who are self-quarantined (Q_2), those individuals who are seriously ill (I), those individuals who are isolated for treatment (T) and recovered population (R). The parameters mentioned in the model (8) are thoroughly defined and their corresponding values are presented in Table 1. In system (8) individuals in (Q_1) compartment, representing susceptible people under quarantine due to lockdown, interact to infected people with a reduced rate compare to individuals in the susceptible (S) compartment. This concept is governed by multiplying a scaling factor σ with the contact rate β , where $0 \leq \sigma \leq 1$ and $1 - \sigma$ represents the effectiveness of lockdown i.e., $\sigma = 0$ describe the scenario of complete lockdown and $\sigma = 1$ describe the situation of no lockdown.

The above classical-integer order model of COVID-19 (8)-(9) is expanded into a fractional order system with an order α ($0 < \alpha \leq 1$). As, the model represented by equations (8) can be expressed in integral form as:

$$\begin{aligned} \frac{dS(t)}{dt} &= \int_0^t \kappa(t-s)[(1-\rho)\Omega - \beta S(A+I) \\ &\quad - (\mu + \lambda)S + \zeta Q_1] ds, \\ \frac{dQ_1(t)}{dt} &= \int_0^t \kappa(t-s)[\rho\Omega - \sigma\beta Q_1(A+I) + \lambda S \\ &\quad - (\mu + \zeta)Q_1] ds, \\ \frac{dA(t)}{dt} &= \int_0^t \kappa(t-s)[\beta S(A+I) + \sigma\beta Q_1(A+I) \\ &\quad - (q_1 + q_2 + \mu)A] ds, \\ \frac{dQ_2(t)}{dt} &= \int_0^t \kappa(t-s)[q_1 A - (q_3 + q_4 + \mu)Q_2] ds, \\ \frac{dI(t)}{dt} &= \int_0^t \kappa(t-s)[q_3 Q_2 + q_2 A \\ &\quad + (\delta + \gamma + \mu)I] ds, \\ \frac{dT(t)}{dt} &= \int_0^t \kappa(t-s)[\gamma I - (\eta + \mu)T] ds, \\ \frac{dR(t)}{dt} &= \int_0^t \kappa(t-s)[q_4 Q_2 + \eta T - \mu R] ds. \end{aligned} \tag{11}$$

In this context, $\kappa(t-s)$ represents the kernel function. On employing the power law of the kernel function as described in [24], we obtain:

$$\kappa(t-s) = \frac{1}{\Gamma(\alpha-1)}(t-s)^{\alpha-2}. \tag{12}$$

Now, on replacing the value of kernel from equation (12) into equation (11) and subsequently using the CFD with order $\alpha - 1$, we obtain:

$$\begin{aligned} {}^{c_0}\mathfrak{D}_t^{\alpha-1} \left[\frac{dS(t)}{dt} \right] &= {}^{c_0}\mathfrak{D}_t^{\alpha-1} {}^{c_0}\mathfrak{J}_t^{\alpha-1} [(1-\rho)\Omega \\ &\quad - \beta S(A+I) - (\mu + \lambda)S + \zeta Q_1], \\ {}^{c_0}\mathfrak{D}_t^{\alpha-1} \left[\frac{dQ_1(t)}{dt} \right] &= {}^{c_0}\mathfrak{D}_t^{\alpha-1} {}^{c_0}\mathfrak{J}_t^{\alpha-1} [\rho\Omega \\ &\quad - \sigma\beta Q_1(A+I) + \lambda S - (\mu + \zeta)Q_1], \\ {}^{c_0}\mathfrak{D}_t^{\alpha-1} \left[\frac{dA(t)}{dt} \right] &= {}^{c_0}\mathfrak{D}_t^{\alpha-1} {}^{c_0}\mathfrak{J}_t^{\alpha-1} [\beta S(A+I) \\ &\quad + \sigma\beta Q_1(A+I) - (q_1 + q_2 + \mu)A], \\ {}^{c_0}\mathfrak{D}_t^{\alpha-1} \left[\frac{dQ_2(t)}{dt} \right] &= {}^{c_0}\mathfrak{D}_t^{\alpha-1} {}^{c_0}\mathfrak{J}_t^{\alpha-1} [q_1 A \\ &\quad - (q_3 + q_4 + \mu)Q_2], \\ {}^{c_0}\mathfrak{D}_t^{\alpha-1} \left[\frac{dI(t)}{dt} \right] &= {}^{c_0}\mathfrak{D}_t^{\alpha-1} {}^{c_0}\mathfrak{J}_t^{\alpha-1} [q_3 Q_2 + q_2 A \\ &\quad + (\delta + \gamma + \mu)I], \\ {}^{c_0}\mathfrak{D}_t^{\alpha-1} \left[\frac{dT(t)}{dt} \right] &= {}^{c_0}\mathfrak{D}_t^{\alpha-1} {}^{c_0}\mathfrak{J}_t^{\alpha-1} [\gamma I - (\eta + \mu)T], \\ {}^{c_0}\mathfrak{D}_t^{\alpha-1} \left[\frac{dR(t)}{dt} \right] &= {}^{c_0}\mathfrak{D}_t^{\alpha-1} {}^{c_0}\mathfrak{J}_t^{\alpha-1} [q_4 Q_2 + \eta T - \mu R]. \end{aligned} \tag{13}$$

Since, ${}^{c_0}\mathfrak{D}_t^{\alpha-1}$, ${}^{c_0}\mathfrak{J}_t^{\alpha-1}$ are inverse operators to each other. Therefore, the COVID-19 model with fractional order of α ($0 < \alpha \leq 1$) is formulated as:

$$\begin{aligned} {}^{c_0}\mathfrak{D}_t^\alpha S(t) &= (1-\rho)\Omega - \beta S(A+I) \\ &\quad - (\mu + \lambda)S + \zeta Q_1, \\ {}^{c_0}\mathfrak{D}_t^\alpha Q_1(t) &= \rho\Omega - \sigma\beta Q_1(A+I) + \lambda S - (\mu + \zeta)Q_1, \\ {}^{c_0}\mathfrak{D}_t^\alpha A(t) &= \beta S(A+I) + \sigma\beta Q_1(A+I) \\ &\quad - (q_1 + q_2 + \mu)A, \\ {}^{c_0}\mathfrak{D}_t^\alpha Q_2(t) &= q_1 A - (q_3 + q_4 + \mu)Q_2, \\ {}^{c_0}\mathfrak{D}_t^\alpha I(t) &= q_3 Q_2 + q_2 A + (\delta + \gamma + \mu)I, \\ {}^{c_0}\mathfrak{D}_t^\alpha T(t) &= \gamma I - (\eta + \mu)T, \\ {}^{c_0}\mathfrak{D}_t^\alpha R(t) &= q_4 Q_2 + \eta T - \mu R, \end{aligned} \tag{14}$$

In the fractional order systems, maintaining dimensional consistency plays a pivotal role, ensuring that the units of measurement on both sides of the equations align smoothly. To achieve this consistency, a practical approach involves adjusting the parameters on the right-hand side of the equations, typically by raising their power to α , as discussed in [25–27]. In this context, our proposed fractional-order model takes the following form:

$$\begin{aligned}
 {}^c_0\mathcal{D}_t^\alpha S(t) &= (1 - \rho^\alpha)\Omega^\alpha - \beta^\alpha S(A + I) \\
 &\quad - (\mu^\alpha + \lambda^\alpha)S + \zeta^\alpha Q_1, \\
 {}^c_0\mathcal{D}_t^\alpha Q_1(t) &= \rho^\alpha\Omega^\alpha - \sigma^\alpha\beta^\alpha Q_1(A + I) + \lambda^\alpha S \\
 &\quad - (\mu^\alpha + \zeta^\alpha)Q_1, \\
 {}^c_0\mathcal{D}_t^\alpha A(t) &= \beta^\alpha S(A + I) + \sigma^\alpha\beta^\alpha Q_1(A + I) \\
 &\quad - (q_1^\alpha + q_2^\alpha + \mu^\alpha)A, \\
 {}^c_0\mathcal{D}_t^\alpha Q_2(t) &= q_1^\alpha A - (q_3^\alpha + q_4^\alpha + \mu^\alpha)Q_2, \\
 {}^c_0\mathcal{D}_t^\alpha I(t) &= q_3^\alpha Q_2 + q_2^\alpha A + (\delta^\alpha + \gamma^\alpha + \mu^\alpha)I, \\
 {}^c_0\mathcal{D}_t^\alpha T(t) &= \gamma^\alpha I - (\eta^\alpha + \mu^\alpha)T, \\
 {}^c_0\mathcal{D}_t^\alpha R(t) &= q_4^\alpha Q_2 + \eta^\alpha T - \mu^\alpha R,
 \end{aligned} \tag{15}$$

with the initial conditions:

$$\begin{aligned}
 S(0) &= S_0 > 0, Q_1(0) = Q_{1,0} \geq 0, A(0) = A_0 \geq 0, \\
 Q_2(0) &= Q_{2,0} \geq 0, I(0) = I_0 \geq 0, \\
 T(0) &= T_0 \geq 0, R(0) = R_0 \geq 0.
 \end{aligned} \tag{16}$$

4. Analytical Study of the Model

In this segment, we discuss certain key properties for the COVID-19 fractional order model(15).

4.1. Non-negativity and boundedness

To prove the positivity of solutions for fractional order model (15), we first discuss the subsequent lemma.

Lemma 1. (Generalized Mean Value Theorem [28]). *Let $\phi(t)$ is continuous on interval $[a, b]$ and ${}^c_0\mathcal{D}_t^\alpha \in C(a, b]$ with $0 < \alpha \leq 1$, then*

$$\begin{aligned}
 \phi(t) &= \phi(a) + \frac{1}{\Gamma(\alpha)} ({}_0D_t^\alpha \phi)(\mathfrak{z})(t - a)^\alpha, \tag{17} \\
 \text{where, } &a \leq \mathfrak{z} \leq t, \forall t \in (a, b].
 \end{aligned}$$

Thus, if ${}_0D_t^\alpha \phi(t) \geq 0, \forall t \in (a, b)$, then ϕ is a non-decreasing function and if ${}_0D_t^\alpha \phi(t) \leq 0, \forall t \in (a, b)$, then ϕ is a non-increasing function.

Theorem 1. (Positivity). *All solutions of the system (15)-(16) are non-negative and are remains in*

$$\mathbb{R}_+^7 = \{ \mathcal{Q}(t); \mathcal{Q}(t) = (S(t), Q_1(t), A(t), Q_2(t), I(t), T(t), R(t)) \in \mathbb{R}^7, \mathcal{Q}(t) \geq 0 \}.$$

Proof. We will prove the non-negativity of solutions for our system (15) by using the Lemma 1. Since,

$$\begin{aligned}
 {}^c_0\mathcal{D}_t^\alpha S|_{S=0} &= (1 - \rho^\alpha)\Omega^\alpha + \zeta^\alpha Q_1 \geq 0, \\
 {}^c_0\mathcal{D}_t^\alpha Q_1|_{Q_1=0} &= \rho^\alpha\Omega^\alpha + \lambda^\alpha S \geq 0, \\
 {}^c_0\mathcal{D}_t^\alpha A|_{A=0} &= \beta^\alpha SI + \sigma^\alpha\beta^\alpha Q_1 I \geq 0, \\
 {}^c_0\mathcal{D}_t^\alpha Q_2|_{Q_2=0} &= q_1^\alpha A \geq 0, \\
 {}^c_0\mathcal{D}_t^\alpha I|_{I=0} &= q_3^\alpha Q_2 + q_2^\alpha A \geq 0, \\
 {}^c_0\mathcal{D}_t^\alpha T|_{T=0} &= \gamma^\alpha I \geq 0, \\
 {}^c_0\mathcal{D}_t^\alpha R|_{R=0} &= q_4^\alpha Q_2 + \eta^\alpha T \geq 0.
 \end{aligned} \tag{18}$$

As, a result $\forall t > 0$, the solutions of the system remain positive and they will remain within \mathbb{R}_+^7 . Also, the vector field consistently directs towards \mathbb{R}_+^7 on each hyperplane encompassing the non-negativity orthant. \square

Theorem 2. (Boundedness). *All solutions of the system (15)-(16) starting in \mathbb{R}_+^7 is bounded.*

Proof. To establish the theorem, we derive the subsequent result from equations (15) as follows:

$$\begin{aligned}
 {}^c_0\mathcal{D}_t^\alpha \mathbb{P}(t) &= {}^c_0\mathcal{D}_t^\alpha S(t) + {}^c_0\mathcal{D}_t^\alpha Q_1(t) + {}^c_0\mathcal{D}_t^\alpha A(t) \\
 &\quad + {}^c_0\mathcal{D}_t^\alpha Q_2(t) + {}^c_0\mathcal{D}_t^\alpha I(t) \\
 &\quad + {}^c_0\mathcal{D}_t^\alpha T(t) + {}^c_0\mathcal{D}_t^\alpha R(t), \\
 &= \Omega^\alpha - \mu^\alpha \mathbb{P}(t) - \delta^\alpha I, \\
 &\leq \Omega^\alpha - \mu^\alpha \mathbb{P}(t).
 \end{aligned}$$

Utilizing the LT of CFD, as discussed in Definition 3, on the above equation, result in

$$\begin{aligned}
 \mathfrak{s}^\alpha \mathcal{L}[\mathbb{P}(t)] - \mathfrak{s}^{\alpha-1} \mathbb{P}(0) &\leq \frac{\Omega^\alpha}{\mathfrak{s}} - \mu^\alpha \mathcal{L}[\mathbb{P}(t)], \\
 \mathcal{L}[\mathbb{P}(t)] [\mathfrak{s}^\alpha + \mu^\alpha] &\leq \frac{\Omega^\alpha}{\mathfrak{s}} + \mathfrak{s}^{\alpha-1} \mathbb{P}(0), \\
 \mathcal{L}[\mathbb{P}(t)] &\leq \frac{\Omega^\alpha}{\mathfrak{s}(\mathfrak{s}^\alpha + \mu^\alpha)} + \frac{\mathfrak{s}^{\alpha-1}}{\mathfrak{s}^\alpha + \mu^\alpha} \mathbb{P}(0), \\
 \mathbb{P}(t) &\leq \frac{\Omega^\alpha}{\mu^\alpha} \mathcal{L}^{-1} \left[\frac{\mu^\alpha}{\mathfrak{s}(\mathfrak{s}^\alpha + \mu^\alpha)} \right] + \mathbb{P}(0) \mathcal{L}^{-1} \left[\frac{\mathfrak{s}^{\alpha-1}}{\mathfrak{s}^\alpha + \mu^\alpha} \right].
 \end{aligned}$$

By using the Definition 4, we get

$$\begin{aligned}
 \mathbb{P}(t) &\leq \frac{\Omega^\alpha}{\mu^\alpha} [1 - E_\alpha(-\mu^\alpha t^\alpha)] + \mathbb{P}(0) [E_\alpha(-\mu^\alpha t^\alpha)] \\
 &\leq \frac{\Omega^\alpha}{\mu^\alpha} - \left(\frac{\Omega^\alpha}{\mu^\alpha} - \mathbb{P}(0) \right) E_\alpha(-\mu^\alpha t^\alpha) \\
 &\leq \frac{\Omega^\alpha}{\mu^\alpha} - c E_\alpha(-\mu^\alpha t^\alpha), \text{ where } c = \frac{\Omega^\alpha}{\mu^\alpha} - \mathbb{P}(0).
 \end{aligned}$$

This indicates that $0 \leq \mathbb{P}(t) \leq \frac{\Omega^\alpha}{\mu^\alpha}$, as $t \rightarrow \infty$. Therefore, as a consequence the total population and the sub populations all are bounded. Thus,

every solution of the model (15)-(16) starts in region \mathbb{R}_+^7 and remains in the region:

$$\mathfrak{A} = \{(S, Q_1, A, Q_2, I, T, R) \in \mathbb{R}_+^7 : S + Q_1 + A + Q_2 + I + T + R \leq \frac{\Omega^\alpha}{\mu^\alpha}\}.$$

□

4.2. Existence and uniqueness of solution

We discuss the existence and uniqueness of the solution for the CFD model (15) by utilizing the Banach fixed point theory [29] in this segment.

Let $\mathbf{B}(\mathcal{J})$ denote a Banach space consisting of continuous real-valued functions defined on the interval $\mathcal{J} = [0, b]$, with the norm specified as:

$$\|(S, Q_1, A, Q_2, I, T, R)\| = \|S\| + \|Q_1\| + \|A\| + \|Q_2\| + \|I\| + \|T\| + \|R\|,$$

where,

$$\begin{aligned} \|S\| &= \sup_{t \in \mathcal{J}} |S(t)|, \quad \|Q_1\| = \sup_{t \in \mathcal{J}} |Q_1(t)|, \\ \|A\| &= \sup_{t \in \mathcal{J}} |A(t)|, \quad \|Q_2\| = \sup_{t \in \mathcal{J}} |Q_2(t)|, \\ \|I\| &= \sup_{t \in \mathcal{J}} |I(t)|, \quad \|T\| = \sup_{t \in \mathcal{J}} |T(t)|, \\ \|R\| &= \sup_{t \in \mathcal{J}} |R(t)|. \end{aligned}$$

Now, consider the DE,

$$\begin{aligned} {}^C_0\mathfrak{D}_t^\alpha \mathcal{Q}(t) &= \mathcal{G}(t, \mathcal{Q}(t)) ; t \in \mathcal{J}, 0 < \alpha \leq 1, \\ \mathcal{Q}(0) &= \mathcal{Q}_0 \geq 0, \end{aligned} \tag{19}$$

where,

$$\begin{aligned} \mathcal{Q}(t) &= (S(t), Q_1(t), A(t), Q_2(t), I(t), T(t), R(t))', \\ \mathcal{Q}(0) &= (S_0, Q_{1,0}, A_0, Q_{2,0}, I_0, T_0, R_0)', \\ \mathcal{G}(t, \mathcal{Q}(t)) &= (\mathcal{G}_1, \mathcal{G}_2, \mathcal{G}_3, \mathcal{G}_4, \mathcal{G}_5, \mathcal{G}_6, \mathcal{G}_7)', \end{aligned}$$

and

$$\begin{aligned} \mathcal{G}_1(t, \mathcal{Q}(t)) &= \Omega^\alpha(1 - \rho^\alpha) - \beta^\alpha S(A + I) \\ &\quad - (\mu^\alpha + \lambda^\alpha)S + \zeta^\alpha Q_1, \\ \mathcal{G}_2(t, \mathcal{Q}(t)) &= \rho^\alpha \Omega^\alpha - \sigma^\alpha \beta^\alpha Q_1(A + I) + \lambda^\alpha S \\ &\quad - (\mu^\alpha + \zeta^\alpha)Q_1, \\ \mathcal{G}_3(t, \mathcal{Q}(t)) &= \beta^\alpha S(A + I) + \sigma^\alpha \beta^\alpha Q_1(A + I) \\ &\quad - (q_1^\alpha + q_2^\alpha + \mu^\alpha)A, \\ \mathcal{G}_4(t, \mathcal{Q}(t)) &= q_1^\alpha A - (q_3^\alpha + q_4^\alpha + \mu^\alpha)Q_2, \\ \mathcal{G}_5(t, \mathcal{Q}(t)) &= q_3^\alpha Q_2 + q_2^\alpha A + (\delta^\alpha + \mu^\alpha + \gamma^\alpha)I, \\ \mathcal{G}_6(t, \mathcal{Q}(t)) &= \gamma^\alpha I - (\eta^\alpha + \mu^\alpha)T, \\ \mathcal{G}_7(t, \mathcal{Q}(t)) &= q_4^\alpha Q_2 + \eta^\alpha T - \mu^\alpha R. \end{aligned}$$

Theorem 3. All the kernels \mathcal{G}_j , where $j = 1, 2, 3, \dots, 7$ fulfills the Lipschitz condition within the Banach space $\mathbf{B}(\mathcal{J})$.

Proof. Consider, $\mathcal{Q}(t), \overline{\mathcal{Q}}(t)$ be two functions, then

$$\begin{aligned} &\|\mathcal{G}_1(t, \mathcal{Q}(t)) - \mathcal{G}_1(t, \overline{\mathcal{Q}}(t))\| \\ &= \|(1 - \rho^\alpha)\Omega^\alpha - \beta^\alpha S(A + I) - (\mu^\alpha + \lambda^\alpha)S \\ &\quad + \zeta^\alpha Q_1 - (1 - \rho^\alpha)\Omega^\alpha + \beta^\alpha \overline{S}(A + I) \\ &\quad + (\mu^\alpha + \lambda^\alpha)\overline{S} - \zeta^\alpha \overline{Q}_1\| \end{aligned}$$

$$\begin{aligned} &= \|-\beta^\alpha(A + I)(S - \overline{S}) - (\mu^\alpha + \lambda^\alpha)(S - \overline{S})\| \\ &\leq |K_1| \|S - \overline{S}\|, \end{aligned}$$

where, $K_1 = -(\beta^\alpha(d_3 + d_5) + \mu^\alpha + \lambda^\alpha)$

and $\|A\| \leq d_3, \|I\| \leq d_5$.

$$\begin{aligned} &\|\mathcal{G}_2(t, \mathcal{Q}(t)) - \mathcal{G}_2(t, \overline{\mathcal{Q}}(t))\| \\ &= \|\rho^\alpha \Omega^\alpha - \sigma^\alpha \beta^\alpha Q_1(A + I) + \lambda^\alpha S \\ &\quad - (\mu^\alpha + \zeta^\alpha)Q_1 - \rho^\alpha \Omega^\alpha + \sigma^\alpha \beta^\alpha \overline{Q}_1(A + I) \\ &\quad - \lambda^\alpha S + (\mu^\alpha + \zeta^\alpha)\overline{Q}_1\| \\ &= \|\sigma^\alpha \beta^\alpha(A + I)(Q_1 - \overline{Q}_1) \\ &\quad - (\mu^\alpha + \zeta^\alpha)(Q_1 - \overline{Q}_1)\| \end{aligned}$$

$$\begin{aligned} &= \|\sigma^\alpha \beta^\alpha(A + I) + (\mu^\alpha + \zeta^\alpha)(Q_1 - \overline{Q}_1)\| \\ &\leq |K_2| \|Q_1 - \overline{Q}_1\|, \end{aligned}$$

where, $K_2 = -(\sigma^\alpha \beta^\alpha(d_3 + d_5) + (\mu^\alpha + \zeta^\alpha))$

and $\|A\| \leq d_3, \|I\| \leq d_5$.

$$\begin{aligned} &\|\mathcal{G}_3(t, \mathcal{Q}(t)) - \mathcal{G}_3(t, \overline{\mathcal{Q}}(t))\| \\ &= \|\beta^\alpha S(A + I) + \sigma^\alpha \beta^\alpha Q_1(A + I) \\ &\quad - (q_1^\alpha + q_2^\alpha + \mu^\alpha)A - \beta^\alpha S(\overline{A} + I) \\ &\quad - \sigma^\alpha \beta^\alpha Q_1(\overline{A} + I) + (q_1^\alpha + q_2^\alpha + \mu^\alpha)\overline{A}\| \\ &= \|\beta^\alpha S(A - \overline{A}) + \sigma^\alpha \beta^\alpha Q_1(A - \overline{A}) \\ &\quad - (q_1^\alpha + q_2^\alpha + \mu^\alpha)(A - \overline{A})\| \\ &\leq |\beta^\alpha| \|S\| + \sigma^\alpha \beta^\alpha \|Q_1\| + (q_1^\alpha + q_2^\alpha + \mu^\alpha) \|A - \overline{A}\| \\ &\leq |K_3| \|A - \overline{A}\|, \end{aligned}$$

where, $K_3 = (\beta^\alpha d_1 + \sigma^\alpha \beta^\alpha d_2 + q_1^\alpha + q_2^\alpha + \mu^\alpha)$

and $\|S\| \leq d_1, \|Q_1\| \leq d_2$.

$$\begin{aligned} &\|\mathcal{G}_4(t, \mathcal{Q}(t)) - \mathcal{G}_4(t, \overline{\mathcal{Q}}(t))\| \\ &= \|q_1^\alpha A - (q_3^\alpha + q_4^\alpha + \mu^\alpha)Q_2 - q_1^\alpha A \\ &\quad + (q_3^\alpha + q_4^\alpha + \mu^\alpha)\overline{Q}_2\| \\ &= \|(q_3^\alpha + q_4^\alpha + \mu^\alpha)(Q_2 - \overline{Q}_2)\| \\ &\leq |K_4| \|Q_2 - \overline{Q}_2\|, \end{aligned}$$

where, $K_4 = -(q_3^\alpha + q_4^\alpha + \mu^\alpha)$.

$$\begin{aligned} & \|\mathcal{G}_5(t, \mathcal{Q}(t)) - \mathcal{G}_5(t, \overline{\mathcal{Q}(t)})\| \\ &= \|q_3^\alpha Q_2 + q_2^\alpha A + (\delta^\alpha + \mu^\alpha + \gamma^\alpha)I - q_3^\alpha Q_2 - q_2^\alpha A \\ &\quad - (\delta^\alpha + \mu^\alpha + \gamma^\alpha)\bar{I}\| \\ &= \|-(\delta^\alpha + \mu^\alpha + \gamma^\alpha)(I - \bar{I})\| \\ &\leq |K_5| \|I - \bar{I}\|, \end{aligned}$$

where, $K_5 = -(\delta^\alpha + \mu^\alpha + \gamma^\alpha)$.

$$\begin{aligned} & \|\mathcal{G}_6(t, \mathcal{Q}(t)) - \mathcal{G}_6(t, \overline{\mathcal{Q}(t)})\| \\ &= \|\gamma^\alpha I - (\eta^\alpha + \mu^\alpha)T - \gamma^\alpha I + (\eta^\alpha + \mu^\alpha)\bar{T}\| \\ &= \|-(\zeta^\alpha + \mu^\alpha)(T - \bar{T})\| \\ &\leq |K_6| \|T - \bar{T}\|, \end{aligned}$$

where, $K_6 = -(\zeta^\alpha + \mu^\alpha)$.

$$\begin{aligned} & \|\mathcal{G}_7(t, \mathcal{Q}(t)) - \mathcal{G}_7(t, \overline{\mathcal{Q}(t)})\| \\ &= \|q_4^\alpha Q_2 + \eta^\alpha T - \mu^\alpha R - q_4^\alpha Q_2 - \eta^\alpha T - \mu^\alpha \bar{R}\| \\ &= \|-\mu^\alpha(R - \bar{R})\| \\ &\leq |K_7| \|R - \bar{R}\|, \end{aligned}$$

where, $K_7 = -\mu^\alpha$.

After adding all the aforementioned equations, we get

$$\begin{aligned} & \|\mathcal{G}(t, \mathcal{Q}(t)) - \mathcal{G}(t, \overline{\mathcal{Q}(t)})\| \\ &\leq \|\mathcal{G}_1(t, \mathcal{Q}(t)) - \mathcal{G}_1(t, \overline{\mathcal{Q}(t)})\| \\ &\quad + \|\mathcal{G}_2(t, \mathcal{Q}(t)) - \mathcal{G}_2(t, \overline{\mathcal{Q}(t)})\| \\ &\quad + \|\mathcal{G}_3(t, \mathcal{Q}(t)) - \mathcal{G}_3(t, \overline{\mathcal{Q}(t)})\| \\ &\quad + \|\mathcal{G}_4(t, \mathcal{Q}(t)) - \mathcal{G}_4(t, \overline{\mathcal{Q}(t)})\| \\ &\quad + \|\mathcal{G}_5(t, \mathcal{Q}(t)) - \mathcal{G}_5(t, \overline{\mathcal{Q}(t)})\| \\ &\quad + \|\mathcal{G}_6(t, \mathcal{Q}(t)) - \mathcal{G}_6(t, \overline{\mathcal{Q}(t)})\| \\ &\quad + \|\mathcal{G}_7(t, \mathcal{Q}(t)) - \mathcal{G}_7(t, \overline{\mathcal{Q}(t)})\| \\ &\leq |K_1| \|S - \bar{S}\| + |K_2| \|Q_1 - \bar{Q}_1\| + |K_3| \|A - \bar{A}\| \\ &\quad + |K_4| \|Q_2 - \bar{Q}_2\| + |K_5| \|I - \bar{I}\| \\ &\quad + |K_6| \|T - \bar{T}\| + |K_7| \|R - \bar{R}\| \\ &\leq K \|\mathcal{Q}(t) - \overline{\mathcal{Q}(t)}\|, \end{aligned}$$

where, $K = \text{Max}\{|K_i|; i = 1, 2, 3, \dots, 7\}$ is the Lipschitz constant of the kernel $\mathcal{G}(t, \mathcal{Q}(t))$. Hence, $\mathcal{G}(t, \mathcal{Q}(t))$ satisfies the Lipschitz condition. \square

Theorem 4. If $\frac{K}{\Gamma(\alpha + 1)} \leq 1$, then the model (15) possesses a unique solution.

Proof. Consider, $\Psi : B \rightarrow B$ be a linear map represented by,

$$\begin{aligned} \Psi(\mathcal{Q}(t)) &= \mathcal{Q}_0(t) + \frac{1}{\Gamma(\alpha)} \int_0^t \frac{1}{(t-s)^{1-\alpha}} \\ &\quad \times \mathcal{G}(s, \mathcal{Q}(s)) ds, \end{aligned}$$

and, $\mathcal{Q}(t), \overline{\mathcal{Q}(t)} \in B$ then, we have

$$\begin{aligned} & \|\Psi(\mathcal{Q}(t)) - \Psi(\overline{\mathcal{Q}(t)})\| \\ &= \left\| \frac{1}{\Gamma(\alpha)} \int_0^t (t-s)^{\alpha-1} (\mathcal{G}(s, \mathcal{Q}(s)) \right. \\ &\quad \left. - \mathcal{G}(s, \overline{\mathcal{Q}(s)})) ds \right\| \\ &\leq \frac{1}{\Gamma(\alpha)} \int_0^t (t-s)^{\alpha-1} \|\mathcal{G}(s, \mathcal{Q}(s)) \\ &\quad - \mathcal{G}(s, \overline{\mathcal{Q}(s)})\| ds \\ &\leq \frac{K \|\mathcal{Q}(s) - \overline{\mathcal{Q}(s)}\|}{\Gamma(\alpha)} \int_0^t (t-s)^{\alpha-1} ds \\ &\leq \frac{Kt^\alpha}{\alpha\Gamma(\alpha)} \|\mathcal{Q}(s) - \overline{\mathcal{Q}(s)}\|. \end{aligned}$$

Thus, Ψ is a contraction, if $\frac{K}{\Gamma(\alpha + 1)} \leq 1$.

Hence, from Banach contraction principle, the fractional order system (15) possesses a unique solution. \square

5. The Reproduction Number and its Sensitivity Analysis

5.1. Reproduction number

Epidemiologically, the basic reproduction number often denoted as \mathbf{R}_0 indicates the average count of new infections originating from one infected individual within a vulnerable population throughout their infectious period. It is a fundamental concept used to measure the potential for disease transmission in a population. If $\mathbf{R}_0 < 1$ then eventually disease will die out from population and if $\mathbf{R}_0 > 1$, the disease will persist and potentially lead to an outbreak. To calculate \mathbf{R}_0 we first determine the Disease Free Equilibrium point (DFE) denoted by (\mathcal{E}_0^*) . Since, Equilibrium points represent the solutions to equation describing the system, at which the variable experiences zero rate of change. Specifically, the disease free equilibrium (DFE) signifies a state where the disease does not persist within the population. By setting

$$\begin{aligned} {}^{c_0}\mathcal{D}_t^\alpha S &= {}^{c_0}\mathcal{D}_t^\alpha Q_1 = {}^{c_0}\mathcal{D}_t^\alpha A = {}^{c_0}\mathcal{D}_t^\alpha Q_2 \\ &= {}^{c_0}\mathcal{D}_t^\alpha I = {}^{c_0}\mathcal{D}_t^\alpha T = {}^{c_0}\mathcal{D}_t^\alpha R = 0, \end{aligned}$$

we calculate the equilibrium points based on the system. Now, applying the necessary conditions involves setting all infectious compartments of the model to zero i.e. $A = Q_2 = I = T = R = 0$.

We obtained the DFE point of the model as follows:

$$\begin{aligned} \mathcal{E}_0^* &= (S_0^*, Q_{1,0}^*, A_0^*, Q_{2,0}^*, I_0^*, T_0^*, R_0^*) \\ &= \left(\frac{\Omega^\alpha(\mu^\alpha(1 - \rho^\alpha) + \zeta^\alpha)}{\mu^\alpha(\lambda^\alpha + \mu^\alpha + \zeta^\alpha)}, \frac{\Omega^\alpha(\mu^\alpha\rho^\alpha + \lambda^\alpha)}{\mu^\alpha(\lambda^\alpha + \mu^\alpha + \zeta^\alpha)}, \right. \\ &\quad \left. 0, 0, 0, 0, 0 \right). \end{aligned}$$

We then apply the next-generation matrix method [30, 31] to evaluate the \mathbf{R}_0 of the model (15). This involves determining the spectral radius of the next generation matrix (\mathcal{FV}^{-1}), in which \mathcal{F} represent the Jacobian of matrix \mathcal{F} (transmission compartment, signifying the appearance of new infections) and \mathcal{V} express the Jacobian of matrix \mathcal{V} (transition compartment) at the DFE point:

$$\mathcal{F} = \begin{bmatrix} \beta^\alpha(S_0^* + \sigma^\alpha Q_0^*) & 0 & \beta^\alpha(S_0^* + \sigma^\alpha Q_0^*) & 0 \\ 0 & 0 & 0 & 0 \\ 0 & 0 & 0 & 0 \\ 0 & 0 & 0 & 0 \end{bmatrix}$$

$$\mathcal{V} = \begin{bmatrix} b_2 & 0 & 0 & 0 \\ -q_1^\alpha & b_3 & 0 & 0 \\ -q_2^\alpha & -q_3^\alpha & b_4 & 0 \\ 0 & 0 & -\gamma^\alpha & b_5 \end{bmatrix}$$

$$\begin{aligned} \mathbf{R}_0 &= \varrho(\mathcal{FV}^{-1}) \\ &= \frac{\beta^\alpha \Omega^\alpha [\sigma^\alpha (\rho^\alpha \mu^\alpha + \lambda^\alpha) + (\zeta^\alpha + \mu^\alpha (1 - \rho^\alpha))]}{\mu^\alpha b_1 b_3 b_2^2} \\ &\quad \times [b_3 b_2 + q_2^\alpha b_2 + q_3^\alpha q_1^\alpha], \end{aligned} \tag{20}$$

where, $b_1 = \mu^\alpha + \zeta^\alpha + \lambda^\alpha$, $b_2 = q_1^\alpha + q_2^\alpha + \mu^\alpha$, $b_3 = q_3^\alpha + q_4^\alpha + \mu^\alpha$, $b_4 = \delta^\alpha + \gamma^\alpha + \mu^\alpha$ and $b_5 = \eta^\alpha + \mu^\alpha$.

5.2. Sensitivity analysis

Sensitivity analysis is crucial for assessing the robustness of model predictions and understanding how the output variable changes concerning variations in input parameters. Within this part, we delve into the sensitivity analysis of \mathbf{R}_0 and the model parameters by utilizing the Normalized Sensitivity Index as discussed in [32]. This method identifies the most influential parameter for \mathbf{R}_0 and their impacts on disease transmission. The normalized forward sensitivity index of a variable to a parameter is the ratio of the relative change in the variable to the relative change in the parameter. as discussed in [33].

Specifically, for the \mathbf{R}_0 concerning the parameter \mathbf{p} , it is calculated as:

$$\varrho_{\mathbf{p}}^{\mathbf{R}_0} = \frac{\partial \mathbf{R}_0}{\partial \mathbf{p}} \times \frac{\mathbf{p}}{\mathbf{R}_0}. \tag{21}$$

Where, the sensitivity index of \mathbf{R}_0 w.r.t parameter \mathbf{p} is positive, if \mathbf{R}_0 increases concerning \mathbf{p} and negative if \mathbf{R}_0 decreases concerning \mathbf{p} .

Table 1. Parameter description and their corresponding values sourced from the relevant literature [22].

Parameters	Biological meaning	Values
Ω	Recruitment rate of susceptible peoples	0.0000421
ρ	Fraction of individuals under quarantine due to the implemented lockdown	0.5
λ	Transmission rate at which Susceptible people moving to Quarantine class(Q_1)	0.5
β	Rate of transmission of infection between individuals	0.07
μ	Mortality rate	0.0000421
ζ	Transmission rate of Quarantine people moving to Susceptible class	0.0715
σ	efficacy factor of lockdown	0.5
q_1	Rate by which Asymptomatic individual move into self-Quarantine class Q_1	0.2
q_2	Rate by which Asymptomatic individual showing the symptoms	0.1428
q_3	Rate at which Self-Quarantine people enters into Infected class	0.21
q_4	Rate by which self-Quarantine people recovers	0.08
γ	Rate by which infected individuals are treated	0.11
η	Rate by which infected people are recovered with medical treatment	0.0917
δ	Disease induced death rate	0.05

Table 2. Sensitivity indices of R_0 .

parameters	indices
Ω	+1
ρ	-3.27412e-05
β	+1
μ	-1.00031
ζ	+0.0972096
σ	+0.777734
q_1	-0.25982
q_2	-0.09752
q_3	+0.08925
q_4	-0.0892
δ	-0.200737
γ	-0.4416
λ	-0.0972096

However, calculating the sensitivity indices of \mathbf{R}_0 explicitly in terms of the model's parameters proves challenging due to the intricate nature of \mathbf{R}_0 . Consequently, we assess the sensitivity indices using the values of parameters provided in Table 1. We obtained sensitivity indices for

\mathbf{R}_0 concerning the thirteen distinct parameters in the model that are displayed in Table 2. Additionally, a visual representation of these numerical sensitivity indices is provided in Figure 1. According to the computed sensitivity indices, a 10% increment in the recruitment rate (Ω), lockdown efficacy factor (σ), and the transmission rate (β) results in a 10%, 7.7%, and 10% increase in the value of \mathbf{R}_0 , respectively. On the contrary,

two-step Lagrange interpolation approach, as detailed in [34–36] to address the fractional order COVID-19 model (15).

From equation (19), we have

$${}^C_0\mathcal{D}_t^\alpha \mathcal{Q}(t) = \mathcal{G}(t, \mathcal{Q}(t)), \quad t \in [0, b], \quad 0 < \alpha \leq 1, \quad \mathcal{Q}(0) = \mathcal{Q}_0, \quad (22)$$

and its solution is

$$\mathcal{Q}(t) = \mathcal{Q}(0) + \frac{1}{\Gamma(\alpha)} \int_0^t (t-s)^{\alpha-1} \mathcal{G}(s, \mathcal{Q}(s)) ds. \quad (23)$$

Let, $h = \frac{T}{n}$, $t_\vartheta = \vartheta h$, $\vartheta = 0, 1, 2, \dots, n \in \mathbb{Z}^+$, then at point $t = t_{\vartheta+1}$, equation (23) becomes

$$\mathcal{Q}(t_{\vartheta+1}) = \mathcal{Q}(0) + \frac{1}{\Gamma(\alpha)} \int_0^{t_{\vartheta+1}} (t_{\vartheta+1} - s)^{\alpha-1} \times \mathcal{G}(s, \mathcal{Q}(s)) ds,$$

which can be expressed as,

$$\mathcal{Q}(t_{\vartheta+1}) = \mathcal{Q}(0) + \frac{1}{\Gamma(\alpha)} \sum_{\varsigma=0}^{\vartheta} \int_{t_\varsigma}^{t_{\varsigma+1}} (t_{\vartheta+1} - s)^{\alpha-1} \times \mathcal{G}(s, \mathcal{Q}(s)) ds. \quad (24)$$

By approximating the function $\mathcal{G}(s, \mathcal{Q}(s))$ over interval $[t_\varsigma, t_{\varsigma+1}]$ by using the Lagrange polynomial,

$$\mathcal{G}(s, \mathcal{Q}(s)) = \frac{s - t_{\varsigma-1}}{t_\varsigma - t_{\varsigma-1}} \mathcal{G}(t_\varsigma, \mathcal{Q}(t_\varsigma)) - \frac{s - t_\varsigma}{t_\varsigma - t_{\varsigma-1}} \mathcal{G}(t_{\varsigma-1}, \mathcal{Q}(t_{\varsigma-1})). \quad (25)$$

Using equation (25) in (24) and then simplifying the integral, we get

$$\begin{aligned} \mathcal{Q}_{\vartheta+1} &= \mathcal{Q}(0) + \frac{h^\alpha}{\Gamma(\alpha + 2)} \sum_{\varsigma=0}^{\vartheta} \left[\mathcal{G}(t_\varsigma, \mathcal{Q}(t_\varsigma)) \right. \\ &\quad \left. ((2 + \vartheta - \varsigma - \alpha)(1 + \vartheta - \varsigma)^\alpha - (\vartheta - \varsigma)^\alpha(2 + \vartheta - \varsigma + 2\alpha)) \right] \\ &\quad + \frac{h^\alpha}{\Gamma(\alpha + 2)} \sum_{\varsigma=0}^{\vartheta} \left[\mathcal{G}(t_{\varsigma-1}, \mathcal{Q}(t_{\varsigma-1})) \right. \\ &\quad \left. ((1 + \vartheta - \varsigma + \alpha)(\vartheta - \varsigma)^\alpha - (1 + \vartheta - \varsigma)^{\alpha+1}) \right]. \end{aligned} \quad (26)$$

Using the aforementioned scheme (26) for numerical solution of our proposed model (15), we get

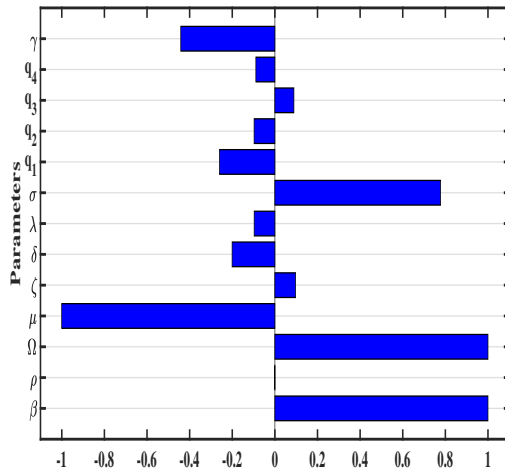


Figure 1. Sensitivity of the \mathbf{R}_0 concerning all thirteen parameters.

when it comes to parameters such as the natural death rate (μ), the treatment rate (γ), the rate at which symptomatic individuals enter self-quarantine (q_1) and disease-induced death rate (δ), an increase of 10% in their values results in a decrease of \mathbf{R}_0 by 4.4%, 2.5%, 2.1%, and 10% respectively.

Therefore, the findings indicate that a 10% rise in the transmission rate β and recruitment rate Ω , significantly increases \mathbf{R}_0 , with a notable impact. Additionally, the lockdown scaling factor σ also demonstrates a substantial effect on \mathbf{R}_0 . While, the remaining parameters exhibit low perturbation, exerting minimal influence on \mathbf{R}_0 . This analysis is depicted in Figure 1, illustrating the high sensitivity of the transmission rate, and the significant impact of the lockdown scaling factor on \mathbf{R}_0 .

6. Numerical Algorithm

We utilize numerical technique to approximate the solutions for nonlinear ordinary and partial differential equations that cannot be resolved through standard analytical techniques. In this study, the numerical approach is based on the

$$\begin{aligned}
S_{\vartheta+1} &= S(0) + \frac{h^\alpha}{\Gamma(\alpha+2)} \sum_{\varsigma=0}^{\vartheta} [\mathcal{G}_1(t_\varsigma, S(t_\varsigma)) \\
&((2 + \vartheta - \varsigma - \alpha)(1 + \vartheta - \varsigma)^\alpha - (\vartheta - \varsigma)^\alpha(2 + \vartheta \\
&- \varsigma + 2\alpha))] + \frac{h^\alpha}{\Gamma(\alpha+2)} \sum_{\varsigma=0}^{\vartheta} [\mathcal{G}_1(t_{\varsigma-1}, S(t_{\varsigma-1})) \\
&((1 + \vartheta - \varsigma + \alpha)(\vartheta - \varsigma)^\alpha - (1 + \vartheta - \varsigma)^{\alpha+1})], \tag{27}
\end{aligned}$$

$$\begin{aligned}
Q_{1,\vartheta+1} &= Q_1(0) + \frac{h^\alpha}{\Gamma(\alpha+2)} \sum_{\varsigma=0}^{\vartheta} [\mathcal{G}_2(t_\varsigma, Q_1(t_\varsigma)) \\
&((2 + \vartheta - \varsigma - \alpha)(1 + \vartheta - \varsigma)^\alpha - (\vartheta - \varsigma)^\alpha(2 + \vartheta \\
&- \varsigma + 2\alpha))] + \frac{h^\alpha}{\Gamma(\alpha+2)} \sum_{\varsigma=0}^{\vartheta} [\mathcal{G}_2(t_{\varsigma-1}, Q_1(t_{\varsigma-1})) \\
&((1 + \vartheta - \varsigma + \alpha)(\vartheta - \varsigma)^\alpha - (1 + \vartheta - \varsigma)^{\alpha+1})], \tag{28}
\end{aligned}$$

$$\begin{aligned}
A_{\vartheta+1} &= A(0) + \frac{h^\alpha}{\Gamma(\alpha+2)} \sum_{\varsigma=0}^{\vartheta} [\mathcal{G}_3(t_\varsigma, A(t_\varsigma)) \\
&((2 + \vartheta - \varsigma - \alpha)(1 + \vartheta - \varsigma)^\alpha - (\vartheta - \varsigma)^\alpha(2 + \vartheta \\
&- \varsigma + 2\alpha))] + \frac{h^\alpha}{\Gamma(\alpha+2)} \sum_{\varsigma=0}^{\vartheta} [\mathcal{G}_3(t_{\varsigma-1}, A(t_{\varsigma-1})) \\
&((1 + \vartheta - \varsigma + \alpha)(\vartheta - \varsigma)^\alpha - (1 + \vartheta - \varsigma)^{\alpha+1})], \tag{29}
\end{aligned}$$

$$\begin{aligned}
Q_{2,\vartheta+1} &= Q_2(0) + \frac{h^\alpha}{\Gamma(\alpha+2)} \sum_{\varsigma=0}^{\vartheta} [\mathcal{G}_4(t_\varsigma, Q_2(t_\varsigma)) \\
&((2 + \vartheta - \varsigma - \alpha)(1 + \vartheta - \varsigma)^\alpha - (\vartheta - \varsigma)^\alpha(2 + \vartheta \\
&- \varsigma + 2\alpha))] + \frac{h^\alpha}{\Gamma(\alpha+2)} \sum_{\varsigma=0}^{\vartheta} [\mathcal{G}_4(t_{\varsigma-1}, Q_2(t_{\varsigma-1})) \\
&((1 + \vartheta - \varsigma + \alpha)(\vartheta - \varsigma)^\alpha - (1 + \vartheta - \varsigma)^{\alpha+1})], \tag{30}
\end{aligned}$$

$$\begin{aligned}
I_{\vartheta+1} &= I(0) + \frac{h^\alpha}{\Gamma(\alpha+2)} \sum_{\varsigma=0}^{\vartheta} [\mathcal{G}_5(t_\varsigma, I(t_\varsigma)) \\
&((2 + \vartheta - \varsigma - \alpha)(1 + \vartheta - \varsigma)^\alpha - (\vartheta - \varsigma)^\alpha(2 + \vartheta \\
&- \varsigma + 2\alpha))] + \frac{h^\alpha}{\Gamma(\alpha+2)} \sum_{\varsigma=0}^{\vartheta} [\mathcal{G}_5(t_{\varsigma-1}, I(t_{\varsigma-1})) \\
&((1 + \vartheta - \varsigma + \alpha)(\vartheta - \varsigma)^\alpha - (1 + \vartheta - \varsigma)^{\alpha+1})], \tag{31}
\end{aligned}$$

$$\begin{aligned}
T_{\vartheta+1} &= T(0) + \frac{h^\alpha}{\Gamma(\alpha+2)} \sum_{\varsigma=0}^{\vartheta} [\mathcal{G}_6(t_\varsigma, T(t_\varsigma)) \\
&((2 + \vartheta - \varsigma - \alpha)(1 + \vartheta - \varsigma)^\alpha - (\vartheta - \varsigma)^\alpha(2 + \vartheta \\
&- \varsigma + 2\alpha))] + \frac{h^\alpha}{\Gamma(\alpha+2)} \sum_{\varsigma=0}^{\vartheta} [\mathcal{G}_6(t_{\varsigma-1}, T(t_{\varsigma-1})) \\
&((1 + \vartheta - \varsigma + \alpha)(\vartheta - \varsigma)^\alpha - (1 + \vartheta - \varsigma)^{\alpha+1})], \tag{32}
\end{aligned}$$

$$\begin{aligned}
R_{\vartheta+1} &= R(0) + \frac{h^\alpha}{\Gamma(\alpha+2)} \sum_{\varsigma=0}^{\vartheta} [\mathcal{G}_7(t_\varsigma, R(t_\varsigma)) \\
&((2 + \vartheta - \varsigma - \alpha)(1 + \vartheta - \varsigma)^\alpha - (\vartheta - \varsigma)^\alpha(2 + \vartheta \\
&- \varsigma + 2\alpha))] + \frac{h^\alpha}{\Gamma(\alpha+2)} \sum_{\varsigma=0}^{\vartheta} [\mathcal{G}_7(t_{\varsigma-1}, R(t_{\varsigma-1})) \\
&((1 + \vartheta - \varsigma + \alpha)(\vartheta - \varsigma)^\alpha - (1 + \vartheta - \varsigma)^{\alpha+1})]. \tag{33}
\end{aligned}$$

7. Results and Discussion

We utilized the numerical method outlined in preceding subsection, and employed baseline values for parameters (as detailed in Table 1) and the initial conditions of the model from pertinent literature [22]. The initial conditions were specified as follows:

$$\begin{aligned}
S(0) &= 0.69 \times 10^9, Q_1(0) = 0.7 \times 10^9, \\
A(0) &= 3800, Q_2(0) = 800, I(0) = 601, \\
T(0) &= 825, R(0) = 566. \tag{34}
\end{aligned}$$

To illustrate the dynamics of the formulated COVID-19 model (15), we provide graphical visualizations in Figures 2, 3, 4 and 5. These visualizations enable us to analyze the influence of the CFD on the dynamics of population by altering key model parameters and exploring different values of fractional order. We used MATLAB software for simulating numerical results, and our discussed numerical approach provided approximate solutions, which are visually depicted in the referenced figures. Figure 2 displays the population dynamics of the discussed model, utilizing the CFD within a time sequence framework, measured in weeks. In Figure 2, the behaviors of $I(t)$, $Q_2(t)$, $T(t)$, and $R(t)$ are portrayed for fractional order values $\alpha = 0.80, 0.85, 0.90, 0.95$ and 1 .

Figure 2a demonstrates that infection increase and decrease rapidly as the fractional order rises.

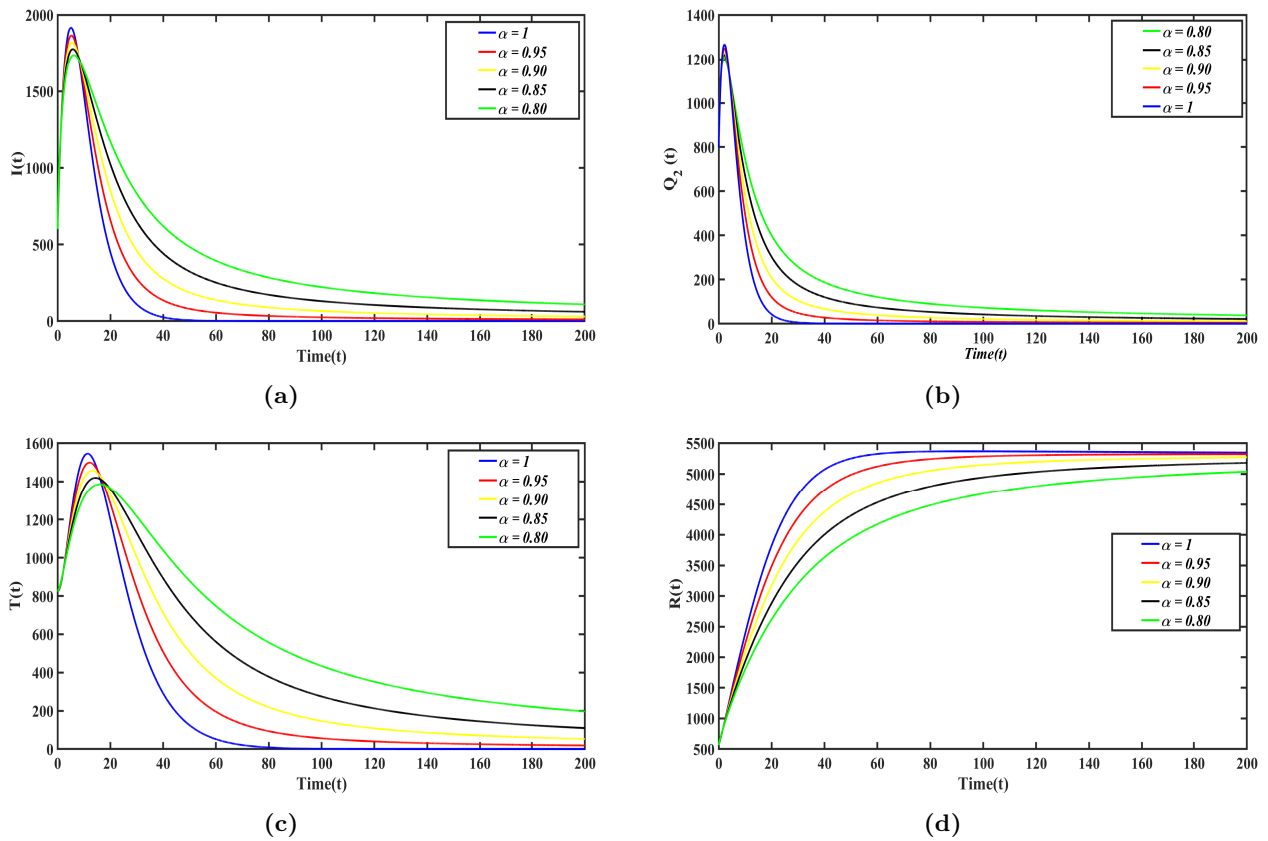


Figure 2. Solution behavior of $I(t)$, $Q_2(t)$, $T(t)$, $R(t)$.

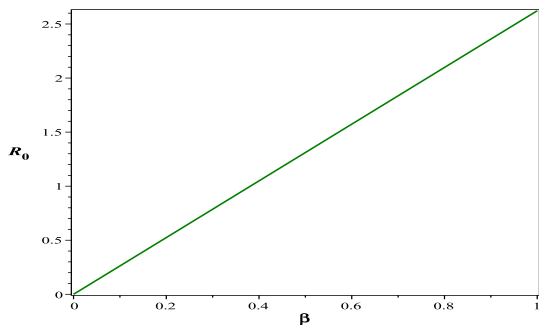
Similar patterns can be observed in Figures 2b and 2c, respectively. During this critical period, medical treatment plays a pivotal role in controlling infections, ensuring suitable care for individuals and facilitating their recovery, as indicated in Figure 2d. The recovered population increases over time, with variations observed for different fractional order values. It is noteworthy that, as α approach to 1, the fractional order model solution converges toward the solution obtained from the conventional integer-order model. The convergence becomes faster as the fractional order α approaches one. This behavior can be attributed to fractional order derivatives retaining the population dynamics of previous time instants, which effectively slows down the rate of reaching stability.

Figures 3, 4 and 5 illustrate the impact of highly sensitive parameters such as β (transmission rate), σ (lockdown scaling factor), and γ (rate of exposure to treatment class) on \mathbf{R}_0 and simultaneously explores the impact of the transmission rate, lockdown scaling factor and recovery rate on the presented model. We investigate how these governing factors influence the dynamics and behavior of the system. The strategies for managing the spread of the disease primarily revolve around minimizing

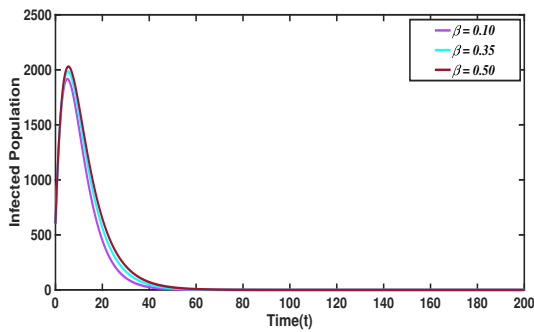
the transmission of the covid-19 infection from individuals who are infected to those who are susceptible, and enhancing the rate of recovery. These measures are crucial in managing and preventing the continued dissemination of the disease. On the left side of the figures, pattern of the (\mathbf{R}_0) is displayed, while the right side illustrates the behavior of the infected population for distinct values of the specified parameters.

Figure 3, illustrates the dynamical behavior of \mathbf{R}_0 and COVID-19-infected individuals under various transmission rates (β), while the remaining parameters remain the same as in Table 1, with considering a fractional order $\alpha = 1$.

It reveals that β leads to a rapid and substantial increase in \mathbf{R}_0 , and as its value escalates from 0.10 to 0.50, result in a corresponding rise in the infection. Figure 4, illustrates the dynamical behavior of \mathbf{R}_0 and COVID-19-infected individuals under various transmission rates (γ), while the remaining parameters remain the same as in Table 1, with considering a fractional order $\alpha = 1$. The variation of \mathbf{R}_0 concerning γ demonstrates an inverse relation. Increasing the value of γ significantly reduces the cases of infected

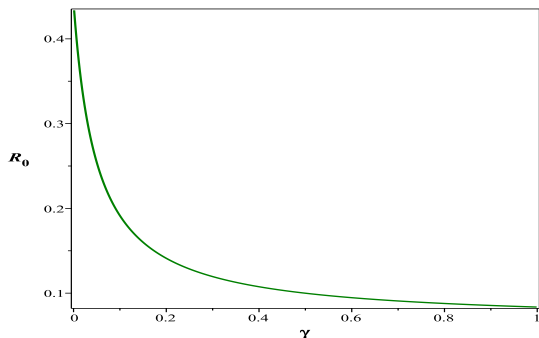


(a)

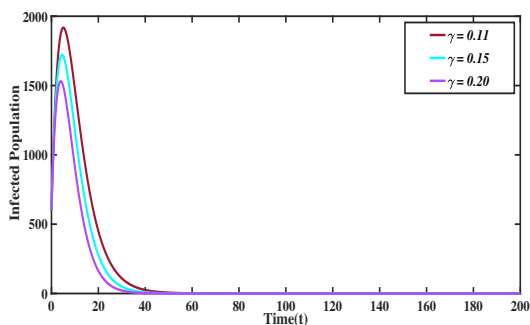


(b)

Figure 3. (a) Variation of R_0 with β . (b) Variation of infected population.



(a)



(b)

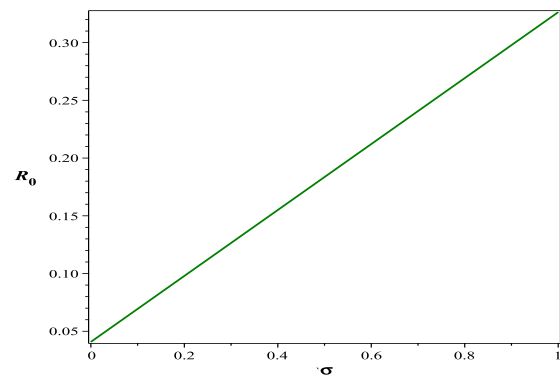
Figure 4. (a) Variation of R_0 with γ . (b) Variation of Infected Population.

individuals, as depicted in Figure 4. Additionally, Figure 5 illustrates the dynamical behavior of R_0 and COVID-19-infected individuals under various transmission rates (β), while the remaining

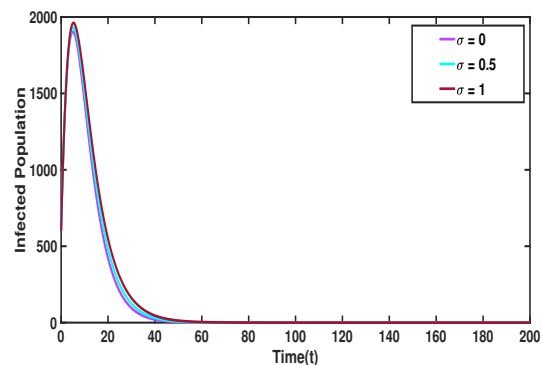
parameters remain the same as in Table 1, with considering a fractional order $\alpha = 1$, where, $\sigma = 0$ corresponds to a state of complete lockdown, $\sigma = 0.5$ to a partial lockdown and, $\sigma = 1$ to a no lockdown scenario. It depicts the impact of the parameter σ on the R_0 and on the infected population, ranging from 0 to 1. It is evident that without imposing a lockdown, infection levels would inevitably rise.

8. Conclusions

In our study, we investigated the mathematical model involving CFD to determine the transmission dynamics of COVID-19. Our analysis included fundamental assessments of the formulated model, ensuring boundedness and non-negativity within the feasible region. These analyses ensure that the model offers valuable and realistic perspective into the dynamics of COVID-19 outbreak. With addition to this, we established the existence and uniqueness of proposed model solutions with the help of Banach fixed



(a)



(b)

Figure 5. (a) Variation of R_0 with σ . (b) Variation of Infected Population.

point theorem. We computed the basic reproduction number R_0 by employing the next-generation matrix technique, serving as

a threshold parameter in the evolution of infection. This parameter is pivotal in identifying whether the disease endures or dissipates within the population. Furthermore, we employed the normalized sensitivity index to conduct a sensitivity analysis of \mathbf{R}_0 for several model parameters. The impact of different parameters on the \mathbf{R}_0 has been analyzed as well. This analysis enabled us to pinpoint the control parameters significantly impacting the progression of infection.

Moreover, we utilized the two-step Lagrange interpolation method to perform numerical simulations across various fractional order values (α) in the proposed fractional model. This numerical approach not only validated our theoretical results but also provided significant insights into the dynamical behavior of the model influenced by fractional order. Our numerical results highlighted the substantial impact of increasing the lockdown scaling factor σ and decreasing the transmission rate β on reducing the number of COVID-19 infections. Furthermore, these findings offer crucial insights for intervention strategies, especially concerning lockdown measures, effectively managing COVID-19 transmission, and reducing the transmission rate. Implementing isolation and quarantining susceptible also emerged as effective strategies to curtail transmission.

While the fractional order COVID-19 model has furnished valuable insights into the epidemic transmission process and identified critical factors for its spread, a more detailed analysis requires extending the model along with some additional factors. Future research work should incorporate various fractional derivatives, such as fractal-fractional, Atangana-Beta derivative, Caputo-Fabrizio, and more. These extensions will pave the way for more comprehensive and in-depth studies in the field.

Acknowledgments

The authors express their sincere thanks to the editor and reviewers for their valuable comments and suggestions that improved the quality of the manuscript.

References


- [1] Bacaër, N. (2011). Mckendrick and kermack on epidemic modelling (1926-1927). *A Short History of Mathematical Population Dynamics*, 89-96. https://doi.org/10.1007/978-0-85729-115-8_16
- [2] Worldometer. *Coronavirus incubation period*. Available from: <https://www.worldometers.info/coronavirus/coronavirus-incubation-period/>.
- [3] Li, M. T., Sun, G. Q., Zhang, J., Zhao, Y., Pei, X., Li, L., & Jin, Z. (2020). Analysis of covid-19 transmission in shanxi province with discrete time imported cases. *Mathematical Biosciences and Engineering*, 17(4), 3710. <https://doi.org/10.3934/mbe.2020208>
- [4] Eikenberry, S. E., Mancuso, M., Iboi, E., Phan, T., Eikenberry, K., Kuang, Y., & Gumel, A. B. (2020). To mask or not to mask: Modeling the potential for face mask use by the general public to curtail the covid-19 pandemic. *Infectious Disease Modelling*, 5, 293-308. <https://doi.org/10.1016/j.idm.2020.04.001>
- [5] Sarkar, K., Khajanchi, S., & Nieto, J. J. (2020). Modeling and forecasting the COVID-19 pandemic in India. *Chaos, Solitons & Fractals*, 139, 110049. <https://doi.org/10.1016/j.chaos.2020.110049>
- [6] Podlubny, I. (1999). *Fractional Differential Equations*, Mathematics in Science and Engineering, Academic Press, New York, NY, USA, 198.
- [7] Sadki, M., Danane, J., & Allali, K. (2023). Hepatitis C virus fractional-order model: mathematical analysis. *Modeling Earth Systems and Environment*, 9(2), 1695-1707. <https://doi.org/10.1007/s40808-022-01582-5>
- [8] Kumawat, S., Bhattar, S., Suthar, D. L., Purohit, S. D., & Jangid, K. (2022). Numerical modeling on age-based study of coronavirus transmission. *Applied Mathematics in Science and Engineering*, 30(1), 609-634. <https://doi.org/10.1080/27690911.2022.2116435>
- [9] Naik, P. A., Yavuz, M., Qureshi, S., Zu, J., & Townley, S. (2020). Modeling and analysis of COVID-19 epidemics with treatment in fractional derivatives using real data from Pakistan. *The European Physical Journal Plus*, 135, 1-42. <https://doi.org/10.1140/epjp/s13360-020-00819-5>
- [10] Asamoah, J. K. K., Okyere, E., Yankson, E., Opoku, A. A., Adom-Konadu, A., Acheampong, E., & Arthur, Y. D. (2022). Non-fractional and fractional mathematical analysis and simulations for Q fever. *Chaos, Solitons & Fractals*, 156, 111821. <https://doi.org/10.1016/j.chaos.2022.111821>
- [11] Naik, P. A., Owolabi, K. M., Yavuz, M., & Zu, J. (2020). Chaotic dynamics of a fractional order HIV-1 model involving AIDS-related cancer cells. *Chaos, Solitons & Fractals*, 140, 110272. <https://doi.org/10.1016/j.chaos.2020.110272>
- [12] Karaagac, B., Owolabi, K. M., & Nisar, K. S. (2020). Analysis and dynamics of illicit drug use described by fractional derivative with Mittag-Leffler kernel. *CMC-Comput Mater Cont*,

- 65(3), 1905-1924. <https://doi.org/10.32604/cm.2020.011623>
- [13] Bhattar, S., Jangid, K., & Purohit, S. D. (2022). Fractionalized mathematical models for drug diffusion. *Chaos, Solitons & Fractals*, 165, 112810. <https://doi.org/10.1016/j.chaos.2022.112810>
- [14] Nazir, G., Zeb, A., Shah, K., Saeed, T., Khan, R. A., & Khan, S. I. U. (2021). Study of COVID-19 mathematical model of fractional order via modified Euler method. *Alexandria Engineering Journal*, 60(6), 5287-5296. <https://doi.org/10.1016/j.aej.2021.04.032>
- [15] Carvalho, A. R., Pinto, C. M., & Tavares, J. N. (2019). Maintenance of the latent reservoir by pyroptosis and superinfection in a fractional order HIV transmission model. *An International Journal of Optimization and Control: Theories & Applications (IJOCTA)*, 9(3), 69-75. <https://doi.org/10.11121/ijocta.01.2019.00643>
- [16] Koca, I. (2018). Analysis of rubella disease model with non-local and non-singular fractional derivatives. *An International Journal of Optimization and Control: Theories & Applications (IJOCTA)*, 8(1), 17-25. <https://doi.org/10.11121/ijocta.01.2018.00532>
- [17] Bhattar, S., Jangid, K., Abidemi, A., Owolabi, K. M., & Purohit, S. D. (2023). A new fractional mathematical model to study the impact of vaccination on COVID-19 outbreaks. *Decision Analytics Journal*, 6, 100156. <https://doi.org/10.1016/j.dajour.2022.100156>
- [18] Owolabi, K. M., & Pindza, E. (2022). A nonlinear epidemic model for tuberculosis with Caputo operator and fixed point theory. *Healthcare Analytics*, 2, 100111. <https://doi.org/10.1016/j.health.2022.100111>
- [19] Naik, P. A., Owolabi, K. M., Zu, J., & Naik, M. U. D. (2021). Modeling the transmission dynamics of COVID-19 pandemic in Caputo type fractional derivative. *Journal of Multiscale Modelling*, 12(03), 2150006. <https://doi.org/10.1142/S1756973721500062>
- [20] Nisar, K. S., Ahmad, S., Ullah, A., Shah, K., Alrabaiiah, H., & Arfan, M. (2021). Mathematical analysis of SIRD model of COVID-19 with Caputo fractional derivative based on real data. *Results in Physics*, 21, 103772. <https://doi.org/10.1016/j.rinp.2020.103772>
- [21] Yıldız, T. A. (2019). A comparison of some control strategies for a non-integer order tuberculosis model. *An International Journal of Optimization and Control: Theories & Applications (IJOCTA)*, 9(3), 21-30. <https://doi.org/10.11121/ijocta.01.2019.00657>
- [22] Bugalia, S., Bajiya, V. P., Tripathi, J. P., Li, M. T., & Sun, G. Q. (2020). Mathematical modeling of COVID-19 transmission: the roles of intervention strategies and lockdown. *Math. Biosci. Eng.*, 17(5), 5961-5986. <https://doi.org/10.3934/mbe.2020318>
- [23] Menaria, N., Purohit, S. D., & Parmar, R. K. (2016). On a new class of integrals involving generalized Mittag-Leffler function. *Surveys in Mathematics and its Applications*, 11, 1-9.
- [24] Wang, J. L., & Li, H. F. (2011). Surpassing the fractional derivative: Concept of the memory-dependent derivative. *Computers & Mathematics with Applications*, 62(3), 1562-1567. <https://doi.org/10.1016/j.camwa.2011.04.028>
- [25] Özköse, F. (2024). Modeling of psoriasis by considering drug influence: A mathematical approach with memory trace. *Computers in Biology and Medicine*, 168, 107791. <https://doi.org/10.1016/j.compbiomed.2023.107791>
- [26] Özköse, F. (2023). Long-term side effects: a mathematical modeling of COVID-19 and stroke with real data. *Fractal and Fractional*, 7(10), 719. <https://doi.org/10.3390/fractalfract7100719>
- [27] Özköse, F., Habbireeh, R., & Şenel, M. T. (2023). A novel fractional order model of SARS-CoV-2 and Cholera disease with real data. *Journal of Computational and Applied Mathematics*, 423, 114969. <https://doi.org/10.1016/j.cam.2022.114969>
- [28] Odibat, Z. M., & Shawagfeh, N. T. (2007). Generalized Taylor's formula. *Applied Mathematics and Computation*, 186(1), 286-293. <https://doi.org/10.1016/j.amc.2006.07.102>
- [29] Lin, W. (2007). Global existence theory and chaos control of fractional differential equations. *Journal of Mathematical Analysis and Applications*, 332(1), 709-726. <https://doi.org/10.1016/j.jmaa.2006.10.040>
- [30] Van den Driessche, P., & Watmough, J. (2002). Reproduction numbers and sub-threshold endemic equilibria for compartmental models of disease transmission. *Mathematical Biosciences*, 180(1-2), 29-48. [https://doi.org/10.1016/S0025-5564\(02\)00108-6](https://doi.org/10.1016/S0025-5564(02)00108-6)
- [31] Martcheva, M. (2015). An introduction to mathematical epidemiology, Springer, 61. https://doi.org/10.1007/978-1-4899-7612-3_1
- [32] Chitnis, N., Hyman, J. M., & Cushing, J. M. (2008). Determining important parameters in the spread of malaria through the sensitivity analysis of a mathematical model. *Bulletin of Mathematical Biology*, 70, 1272-1296. <https://doi.org/10.1007/s11538-008-9299-0>
- [33] Mishra, A. M., Purohit, S. D., Owolabi, K. M., & Sharma, Y. D. (2020). A nonlinear epidemiological model considering asymptotic and quarantine classes for SARS CoV-2 virus. *Chaos, Solitons & Fractals*, 138, 109953. <https://doi.org/10.1016/j.chaos.2020.109953>
- [34] Diethelm, K., & Freed, A. D. (1998). The FracPECE subroutine for the numerical solution of differential equations of fractional order.


Forschung und wissenschaftliches Rechnen, 1999, 57-71.

- [35] Diethelm, K., Ford, N. J., & Freed, A. D. (2004). Detailed error analysis for a fractional Adams method. *Numerical Algorithms*, 36, 31-52. <https://doi.org/10.1023/B:NUMA.0000027736.85078.be>
- [36] Atangana, A., & Owolabi, K. M. (2018). New numerical approach for fractional differential equations. *Mathematical Modelling of Natural Phenomena*, 13(1), 3. <https://doi.org/10.1051/mmnp/2018010>

Sanjay Bhatner is an assistant professor of mathematics in the Department of Mathematics, Malaviya National Institute of Technology, Jaipur, Rajasthan, India. His research interests include Special Functions, Fractional Calculus, Mathematical Modeling, Integral Transforms, and Integral Inequalities.


 <https://orcid.org/0000-0003-1717-2178>

Sangeeta Kumawat received graduation degree from S.S. Jain Subodh P.G. Autonomous College, Jaipur, India and M.Sc. degree from Central University of Rajasthan, India. Currently, She is a research scholar at Department of Mathematics, Malaviya National Institute of Technology, Jaipur, India. Her research interests include Mathematical Modelling and Fractional Calculus.


 <https://orcid.org/0009-0002-2434-6930>

Bhamini Bhatia received graduation degree from Tagore Aadarsh P.G. College, Jaipur, India and

M.Sc. degree from JECRC University, Jaipur, India. Currently, She is a research scholar at Department of Mathematics, Malaviya National Institute of Technology, Jaipur, India. Her research interests include Mathematical Modelling and Fractional Calculus.

 <https://orcid.org/0009-0004-6068-2733>

Sunil Dutt Purohit obtained his M.Sc. (Gold Medalist) and Ph.D. degree from the faculty of science at Jai Narayan Vyas University, Jodhpur, India. He also had a Joiner and Senior Research Fellowship of Council of Scientific and Industrial Research (CSIR) and then worked in the Department of Mathematics and Statistics, Jai Narayan Vyas University, Jodhpur. After that he joint as Assistant Professor and Head, Department of Basic Sciences, Maharana Pratap University of Agriculture & Technology, Udaipur, India. Currently, he is Associate Professor of Mathematics, Department of HEAS (Mathematics), Rajasthan Technical University, Kota. His research interest includes Special functions, Fractional Calculus, Integral transforms, Basic Hypergeometric Series, Geometric Function Theory and Mathematical Physics. He has published more than 120 research papers in international esteemed journals. He is reviewer for *Mathematical Reviews, USA (American Mathematical Society)* and *Zentralblatt MATH, Berlin* since last six years. He is member, Editorial Board for number of international mathematical and interdisciplinary journals.

 <https://orcid.org/0000-0002-1098-5961>

An International Journal of Optimization and Control: Theories & Applications (<http://www.ijocta.org>)



This work is licensed under a Creative Commons Attribution 4.0 International License. The authors retain ownership of the copyright for their article, but they allow anyone to download, reuse, reprint, modify, distribute, and/or copy articles in IJOCTA, so long as the original authors and source are credited. To see the complete license contents, please visit <http://creativecommons.org/licenses/by/4.0/>.